A Mechanism for the Recurrence of Wintertime Midlatitude SST Anomalies

MICHAEL A. ALEXANDER AND CLARA DESER

CIRES, University of Colorado, Boulder, Colorado

(Manuscript received 5 March 1993, in final form 17 June 1994)

ABSTRACT

In the early 1970s, Namias and Born speculated that ocean temperature anomalies created over the deep mixed layer in winter could be preserved in the summer thermocline and reappear at the surface in the following fall or winter. This hypothesis is examined using upper-ocean temperature observations and simulations with a mixed layer model. The data were collected at six ocean weather stations in the North Atlantic and North Pacific. Concurrent and lead–lag correlations are used to investigate temperature variations associated with the seasonal cycle in both the observations and the model simulations.

Concurrent correlations between the surface and subsurface temperature anomalies in both the data and the model indicate that the penetration of temperature anomalies into the ocean is closely tied to the seasonal cycle in mixed layer depth: high correlations extend to relatively deep (shallow) depths in winter (summer). Lead–lag correlations in both the data and the model, at some of the stations, indicate that temperature anomalies beneath the mixed layer in summer are associated with the temperature anomalies in the mixed layer in the previous winter/spring and following fall/winter but are unrelated or weakly opposed to the temperature anomalies in the mixed layer in summer. These results suggest that vertical mixing processes allow ocean temperature anomalies created over a deep mixed layer in winter to be preserved below the surface in summer and reappear at the surface in the following fall, confirming the Namias–Born hypothesis.

1. Introduction

In midlatitudes, departures in the sea surface temperature (SST) from the monthly and seasonal means strongly depend on local air–sea interactions (Gill and Niiler 1973; Frankignoul 1985). The lag correlation analyses of Davis (1976), Lanzante (1984), Wallace and Jiang (1987), and Zorita et al. (1992) and the coupled atmosphere–ocean model simulations of Salmon and Henderschott (1976) and Alexander (1992) indicate that in the extratropics the atmosphere tends to drive the ocean. Anomalous atmospheric forcing can cause SST anomalies to form by wind-driven vertical and horizontal motions associated with Ekman pumping and transport, surface energy fluxes, diffusion, and vertical mixing due to turbulence. Over most of the midlatitude oceans SSTs appear to be controlled primarily by surface fluxes and the entrainment of water from the thermocline into the surface mixed layer (Frankignoul and Reynolds 1983; Frankignoul 1985; Haney 1985; Luksch et al. 1990).

While there is strong evidence that in midlatitudes the atmosphere forces the ocean, the developing ocean anomalies may feed back on the atmosphere. Several studies have indicated that midlatitude SSTs influence the evolution of the atmospheric circulation in certain seasons (Davis 1978; Walsh and Richman 1981; Palmer and Sun 1985; Pitcher et al. 1988; Wallace et al. 1990; Lau and Nath 1990; Kushnir and Lau 1992). To the extent that midlatitude air–sea interaction determines a significant part of the seasonal climate anomalies, a better understanding of the processes that form and maintain SST anomalies may aid in our ability to make seasonal climate predictions.

Ocean temperature anomalies in the surface mixed layer (20–300 m) can be sustained for several months due to the large heat capacity of seawater. At some locations, temperature anomalies that form at the surface of the ocean propagate downward into subsurface layers where they can last for several years (White and Walker 1974). Thus, the potential exists for heat content anomalies stored within the upper ocean to return to the surface and influence the atmospheric circulation in subsequent seasons.

Namias and Born (1970, 1974) and Wallace and Jiang (1987) noted a tendency for midlatitude SST anomalies to recur from one winter to the next without persisting through the intervening summer. Namias and Born speculated that temperature anomalies that form at the surface and extend downward into the deep ocean mixed layer in winter could remain intact in the seasonal thermocline during the following summer. The anomalies would be insulated from surface processes by the reformed, shallow mixed layer and could then reappear at the surface when the mixed layer again deepened in the following fall/winter. A schematic de-

Corresponding author address: Dr. Michael A. Alexander, University of Colorado, CIRES, Campus Box 449, Boulder, CO 80309-0449.

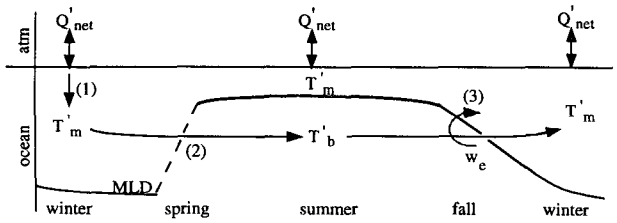

FIG. 1. Schematic diagram of the Namias and Born hypothesis. 1) Anomalous atmospheric forcing (Q'_{net}) in winter creates a temperature anomaly (T'_m) over a deep mixed layer; 2) the temperature anomaly remains beneath the mixed layer (T'_b) when the mixed layer reforms (dashed line) close to the surface in spring; 3) the sub-mixed layer temperature anomaly is entrained (w_e) into the mixed layer in the following fall/winter, influencing the surface temperature.

piction of this re-emergence mechanism is shown in Fig. 1.

In the present study we test the Namias–Born hypothesis using upper-ocean temperature observations from six ocean weather stations located in the North Atlantic (C, D, E, H) and the North Pacific (P, N). We have also performed a number of simulations using a one-dimensional mixed layer model (MLM) at two of the OWSs. The purpose of the MLM experiments is to isolate the reemergence mechanism in simulations with idealized surface forcing and evaluate the influence of surface fluxes and entrainment on the ocean temperature anomalies over the course of the seasonal cycle. For the Namias–Born mechanism to occur the surface flux anomalies must exceed the heat flux anomalies due to entrainment in late winter/early spring and vice versa in the following fall/winter; a MLM is the simplest model that contains these two key physical processes. Additionally, many 1D upper-ocean models have been tested by comparing the simulated SST and mixed layer depth to observations. The ability of the MLM to reproduce the full upper-ocean temperature structure and more specifically, the temperature anomaly patterns associated with the re-emergence mechanism, provides additional tests of the model.

The subsurface temperature data, described in section 2, are analyzed via concurrent and lead–lag correlation analyses in section 3. The mixed layer model, which follows the formulation of Gaspar (1988), is described in section 4. The model is used in idealized experiments (section 5a); extended simulations that attempt to reproduce actual conditions at Ocean Weather Station C in the North Atlantic and P in the North Pacific (section 5b); and studies that examine the sensitivity of the reemergence mechanism to how the surface fluxes and sub-mixed layer diffusion are calculated (section 5c). The results are summarized and discussed in section 6.

2. Data

The upper-ocean temperature observations used in this study were collected at four OWSs in the North Atlantic and two in the North Pacific (Fig 2). The Atlantic and Pacific data were provided by the National Center for Atmospheric Research (NCAR) and the National Oceanographic Data Center (NODC), respectively. All of the data had originally been quality controlled at NODC. The temperature measurements, obtained from mechanical bathythermograph (MBT) casts, were recorded at 5-m increments from the surface to a maximum depth of 270 m, although the deepest observation at many of the stations prior to 1961 was 135 m. The six stations, their locations, the number of reports, and the periods of record are given in Table 1. From 1974 to 1982 expendable rather than mechanical BTs were usually employed to obtain temperature profiles at the OWSs, but due to erratic data collection, information from expendable BTs was not included in the present study.

Monthly temperature anomalies (T'), the primary variable analyzed in the present study, are calculated as follows. First, monthly means are computed by averaging the temperature values within the individual months and then averaging all of the same months over the years spanning the data record. Then daily means are derived by fitting a cubic spline to the

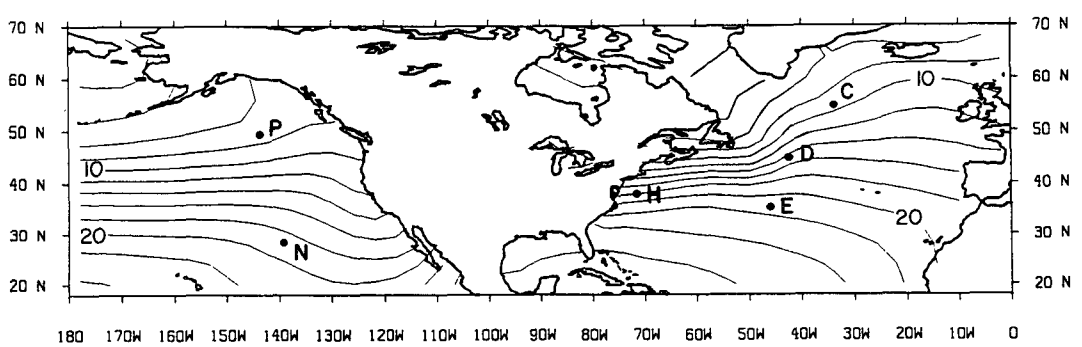

FIG. 2. The locations of the ocean weather stations used in this study, superimposed on the annual average SST field in the North Atlantic and eastern North Pacific.

TABLE 1. The location of the ocean weather stations and the total number of reports, first and last month of data that is used, total number of months with data, and the number of months in which data has been collected to 270 m.

Station	Latitude	Longitude	Number of reports	First month	Last month	Total number of months	Number of months with data to 270 m
C	52°45'N	35°30'W	12 689	Jun 1950	Feb 1973	184	89
D	44°N	41°W	16 160	Oct 1952	Aug 1972	188	86
E	35°N	48°W	16 923	Jan 1953	Jul 1972	185	95
H	38°N	71°W	4006	Jul 1951	Jan 1972	198	78
N	30°N	140°W	13 673	Oct 1950	Jan 1973	218	113
P	50°N	145°W	14 344	May 1950	Jul 1974	264	209

monthly means assuming that they occur in the middle of each month. Anomalies, computed from the difference between individual observations and the corresponding daily means are then averaged over the course of a month to obtain T'. Monthly anomalies are computed in this fashion to avoid biases when the majority of the observations are collected near the beginning or end of a month. The monthly mean and anomalies are smoothed using a 1–2–1 time filter, except in the lead–lag correlation analyses where a 3-month running mean is used.

Ocean Weather Stations C and E in the central North Atlantic, and N and P in the eastern North Pacific are located away from major oceanic fronts and strong current systems, while stations D and H reside within the Gulf Stream (Fig. 2). An examination of the mean and anomalous thermal structure at the six stations indicated that conditions at D and H appear to be different from those at the other four stations. In addition, the analyses were hampered by the lack of data below 135 m at D, which has a very deep mixed layer in winter, and the relatively few number reports at H (Table 1). Therefore, we will focus on the results from P and N in the North Pacific and C and E in the North Atlantic.

We use correlation analyses to characterize the dependence of the temperature variations at the OWSs on depth and season. The structure of the correlation patterns are emphasized insofar as they reflect physical processes. Because the data records are relatively short (ranging from 14 years at E to 23 years at P), large correlation values are required for statistical significance. As a rough guide to statistical significance, correlation coefficient magnitudes > 0.4 at P and N, and >0.5 at C and E, are statistically significant at the 5% level, using a one-tailed Student's t-test and taking into account the autocorrelation in the data according to Leith (1973).

3. Thermal variability at the OWSs

The mean seasonal cycle of ocean temperature and mixed layer depth (MLD) at OWSs P, C, N, and E are shown in Fig. 3. Following Levitus (1982), the MLD, indicated by a star in the plots, is defined as the level at which the temperature is more than 0.5°C colder than the SST. At all four stations a nearly uniform cold deep mixed layer, extending from the surface to about 125–200 m, occurs during late winter. The mixed layer re-forms closer to the surface in spring, with minimum depths of ~25–40 m occurring in July. The maximum surface temperature tends to occur 1 to 2 months after the minimum MLD is reached. A seasonal thermocline, where the temperature decreases rapidly with depth, forms in summer between the base of the mixed layer and approximately 100 m. In contrast, the base of the mixed layer is poorly defined in late winter at P, C, and E as the thermal gradient is weak throughout the upper ocean. At N the MLD is constrained by the relatively strong permanent thermocline, which begins at ~125 m. The mixed layer is deeper in winter at the Atlantic stations, leading to a larger annual range in MLD, compared to the Pacific stations.

Correlation coefficients (r) between concurrent monthly surface and subsurface temperature anomalies are shown in Fig. 4. The correlation values are only displayed down to 135 m due to the limited number of months with data below this depth (Table 1). High correlation values, associated with relatively uniform temperature anomalies within the mixed layer, extend to much greater depths in winter compared with summer, indicative of the seasonal cycle in MLD. For example, at P, correlation coefficients between SST′ and T' in excess of 0.8 extend below 100 m during March but remain above 25 m in August. The mixed layer shoals later in spring and deepens earlier in fall at the Atlantic compared with the Pacific stations (Fig. 3), leading to high correlation values at C and E that extend beyond 135 m except during summer; while at P and N the correlations slowly increase with depth during the fall (Fig. 4).[1]

In late summer the temperature anomalies below the mixed layer exhibit negative correlations (−0.2

[1] The year-to-year standard deviation (σ) of T' (not shown) has a different structure at the Pacific and Atlantic OWSs. At P and N, the maximum σ values, which range from 0.8° to 1.0°C, occur in the surface layer during summer and early fall. In contrast, minimum σ values at C and E, of between 0.4° and 0.6°C, are located in the mixed layer during summer.

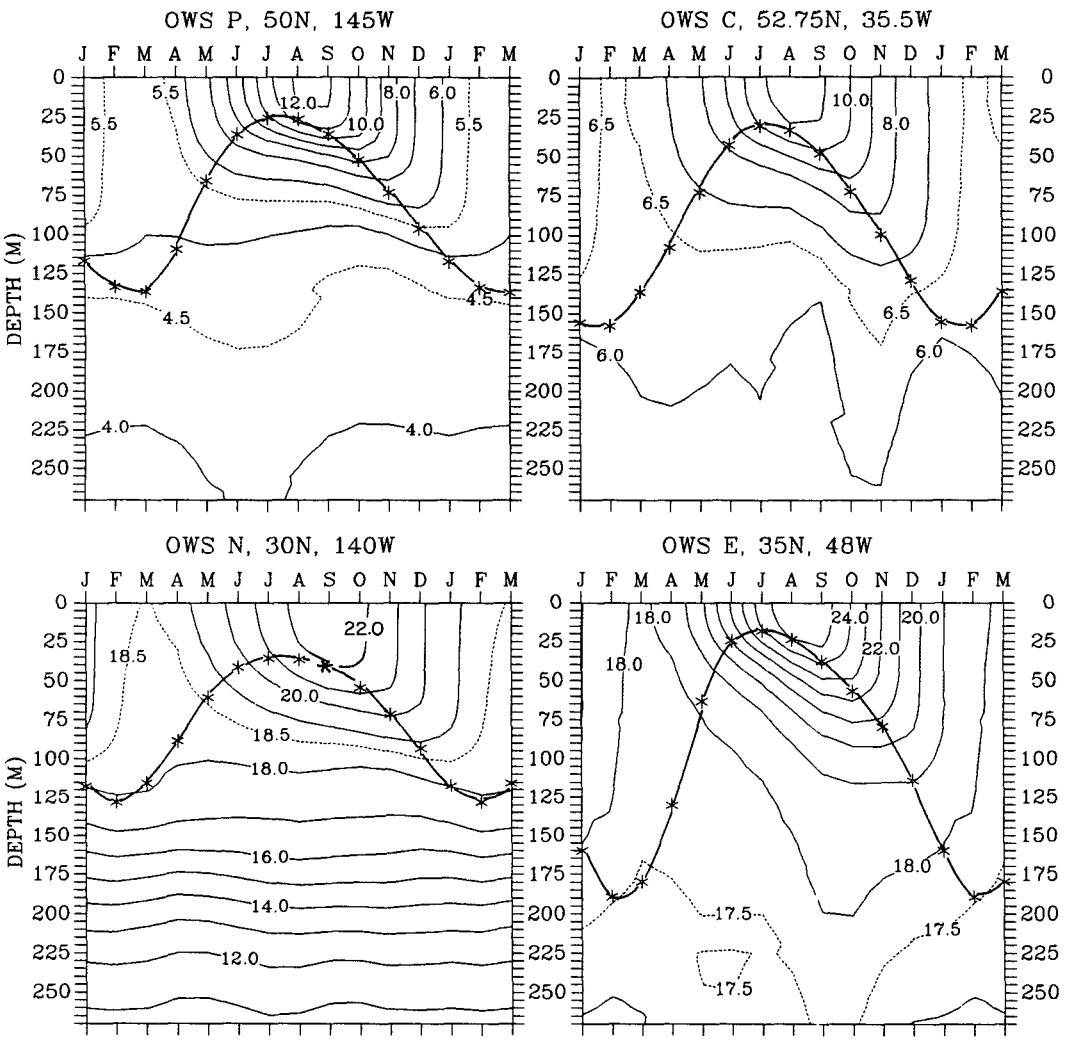

FIG. 3. The mean seasonal cycle of temperature (°C) in the upper 270 m of the ocean and the mixed layer (*) observed at OWS P, C, N, and E. The MLD is determined by finding the depth at which the SST $- T_{depth} > 0.5$°C. Note that the first three months of the year are repeated in order to clearly display the seasonal cycle.

$< r < 0.0$) with the concurrent SST anomalies at all four stations. However, the correlation values are only slightly negative, indicating a relatively weak relationship between T' in the mixed layer and the seasonal thermocline. The negative correlation likely results from the influence of mixed layer and/or seasonal thermocline temperature anomalies on the static stability, and thus the amount of vertical mixing. For example, anomalous heating of the ocean by surface fluxes during summer will cause the mixed layer to be warmer than normal and enhance the static stability. As a result, the mixed layer will be shallower than usual and less warm water will penetrate into the seasonal thermocline. Thus, there is a tendency for an anomalously warm mixed layer to be associated with an anomalously cold thermocline, and vice versa.

In general, high correlation values between SST′ and T' at depth (Fig. 4) extend deeper into the ocean in late spring and fall compared with the monthly mean mixed layer depth (Fig 3). For example, at C, values of $r > 0.8$ extend below 135 m in May, while the MLD is estimated to only be ~75 m. This apparent discrepancy may be related to the intramonthly variability of the mixed layer, especially in spring. During spring the mixed layer re-forms at a relatively shallow depth on warm days with light winds, but storm-generated turbulence can act to re-establish a deep mixed layer. Thus, the monthly average MLD may be somewhere between these extremes, but the correlations between SST′ and T' with depth will reflect the influence of strong mixing events. In addition, the MLD is poorly defined and difficult to estimate in late winter and early spring as the temperature jump across the base of the mixed layer is small.

Lagged correlations between SST′ in April at P, N, and E (February at C) and T' at depth over the follow-

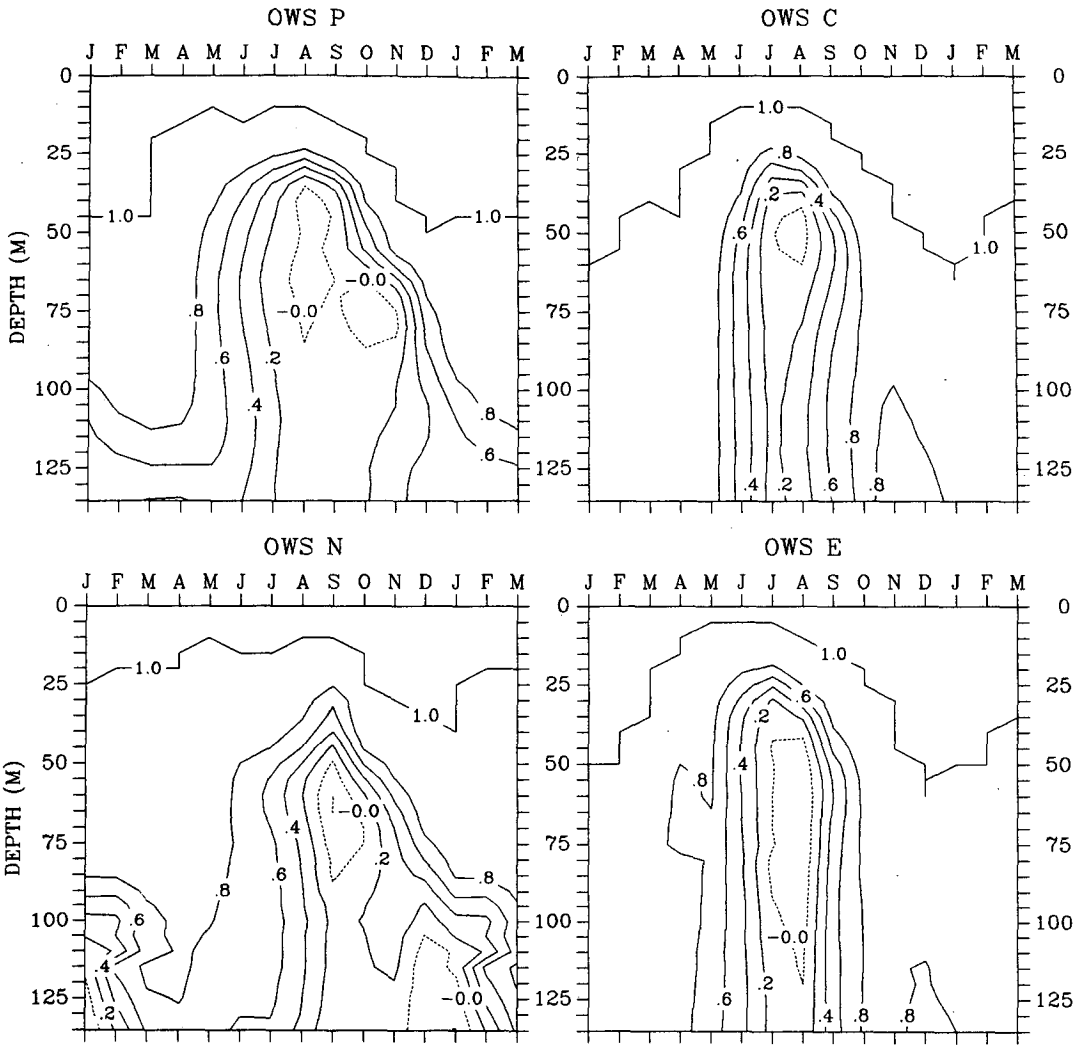

FIG. 4. Concurrent correlations between monthly anomalies of SST and temperatures from the surface to 135 m at 5-m increments at OWS P, C, N, and E. For example, at OWS P the correlation value between SST′ and T' at 125 m during May is 0.6. Note that the first three months of the year are repeated.

ing 16 months are shown in Fig. 5. The data have been smoothed using a 3-month running mean. The surface correlations exhibit a monotonic decrease from the base period (lag = 0) to 4–7 months lag, reaching minimum values of ~ -0.35 to 0.2. This decrease in the autocorrelation of the SST anomaly is primarily due to the damping of ocean temperature anomalies by air–sea feedback (Frankignoul and Hasselman 1977; Frankignoul and Reynolds 1983; Alexander 1992). In contrast, higher correlation values occur at longer lags at depth. For example, correlations between SST′ in the base period and T' exceed $\sim$0.5 below 40 m at 4-months lag at all four stations. The higher correlations beneath the mixed layer in summer likely result from anomalies created in the surface layer in late winter/early spring persisting in the quiescent water within the summer thermocline.

The correlation patterns in Fig. 5 also suggest a connection between temperature anomalies in the surface layer from winter/spring to the following fall/winter via the summer thermocline. At all four stations the correlation values begin to increase in the surface layer in fall or winter after the summer minimum. However, with the exception of C, the correlations between SST′ in spring and the following winter are small ($r < 0.4$). These low correlation values may reflect the influence of net surface heat flux anomalies that are out of phase between winter/spring and the following fall/winter and other processes that obscure the influence of entrainment of subsurface temperature anomalies.

To isolate the relationship between temperature anomalies beneath the mixed layer in summer and temperature anomalies within the mixed layer in the previous and following seasons, we have computed

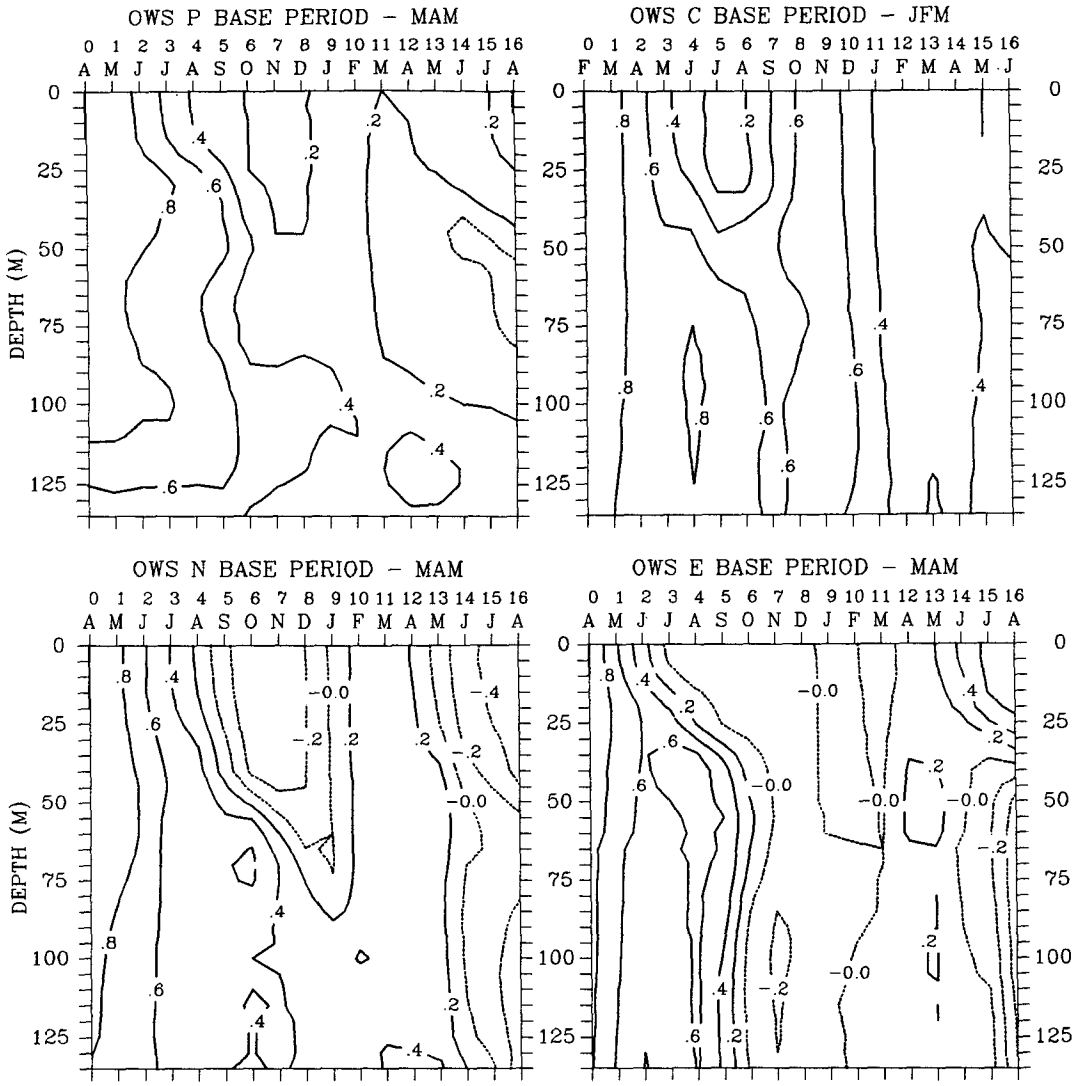

FIG. 5. Lag correlations between the SST anomaly during April at P, N, and E (February at C) and the monthly temperature anomalies at 5-m depth increments from 0 to 16 months lag. The data have been smoothed using a 3-month running mean; the middle month of the 3-month mean is shown at the top of each panel. For example, at N the correlation value between SST′ in April and the T' at 60 m in November (7 months lag) is −0.2.

lead–lag correlations using temperature in the summer thermocline as the base point. Figure 6 shows the correlations between T' at a fixed level in the seasonal thermocline during summer, and T' from the surface to 135 m for the previous and following eight months. The variability in mixed layer structure (see Figs. 2 and 3) leads to the selection of different base points at the four OWSs: 50 m in August at P; 80 m in JAS at C; 75 m during September at N; and 50 m in July at E. At P, high correlation values ($r > 0.6$) extend from the surface down to ~100 m in the previous spring. During summer, T' at 50 m and anomalies in the surface layer have a slight negative correlation, indicating that anomalies in the seasonal thermocline are unrelated or weakly opposed to those in the mixed layer. The correlations near the surface at P increase from summer to the following winter, reaching a maximum of 0.45 during January. The correlation values are generally larger at C compared with P. Remarkably, the correlation between T' at 80 m in August, the base point, and SST′ in December exceeds 0.8 at C. At N and E the maximum negative correlation in the mixed layer occurs 1–2 months after the base period: as the mixed layer deepens in the fall and entrainment increases, the correlation values in the surface layer begin to increase and reach a maximum in the early part of the following year. While the details of the anomaly correlation structures differ, the general pattern at the four stations suggest that temperature anomalies that form in late winter/early spring are stored beneath the

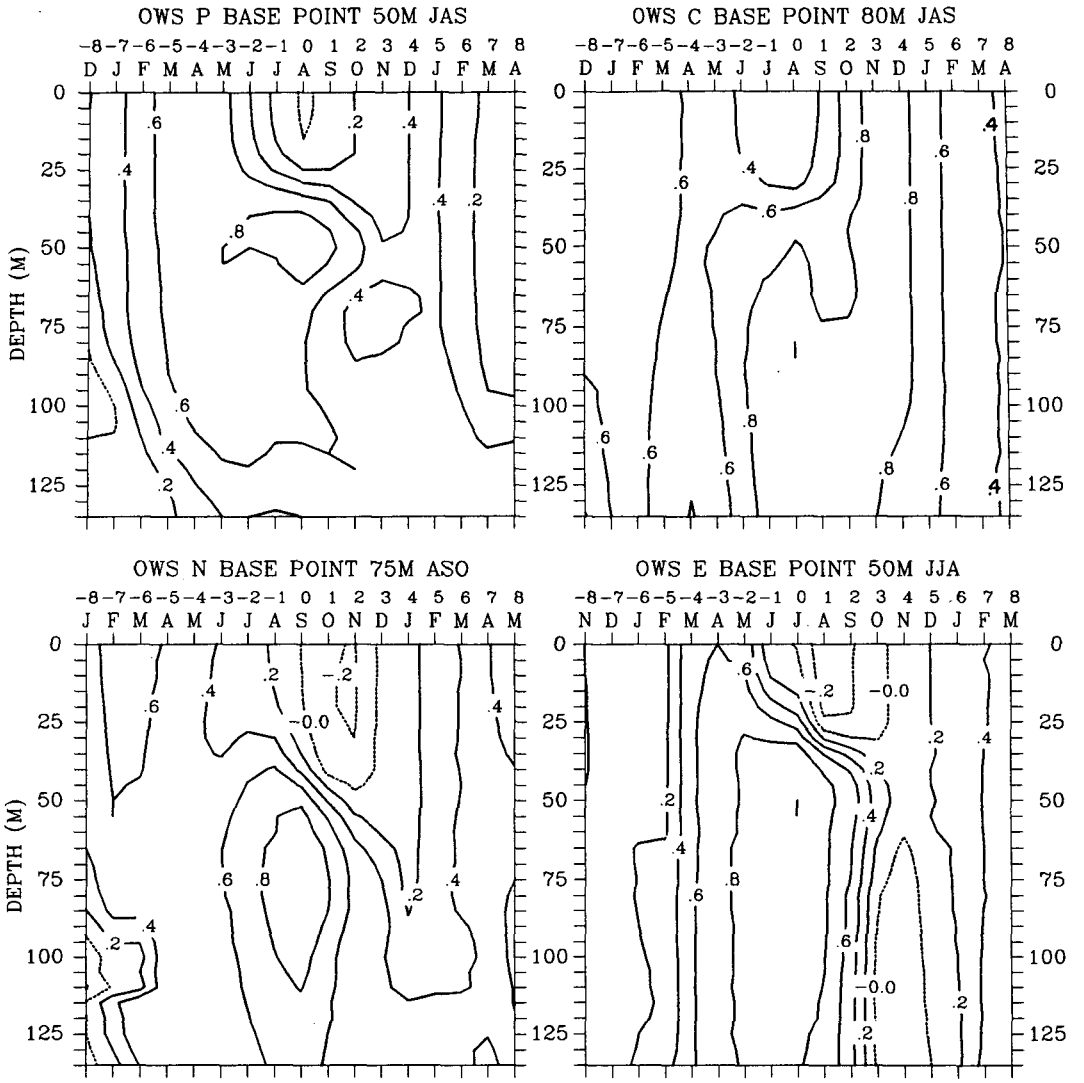

FIG. 6. Lead–lag correlations between the temperature anomaly beneath the summer mixed layer (base point) and temperature anomalies in 5 m increments for the previous and following eight months. The data have been smoothed using a 3-month running mean; the middle month of the 3-month mean is shown at the top of each panel. The base points at the four OWSs are 50 m in August at P; 80 m in August at C; 75 m during September at N and 50 m in July at E. For example, at E the correlation between T' at the surface during April (a 3 month lead) and 50 m in July is 0.6.

surface in summer and are re-entrained into the mixed layer during the following fall and winter, the crux of the Namias–Born hypothesis.

4. Mixed layer ocean model

The near-surface layer of much of the world's oceans is vertically well mixed with nearly uniform temperature and salinity. Variability in mixed layer temperatures can result from vertical processes, including surface energy fluxes and the entrainment of denser water through the base of the mixed layer, and horizontal processes, such as advection and diffusion. Vertical rather than horizontal processes appear to dominate in the development of SST anomalies in the extratropics away from continents and water mass boundaries (Gill and Niiler 1973; Haney et al. 1983; Frankignoul 1985). Ocean model simulations by Haney (1980, 1985), Luksch et al. (1990), and Luksch and von Storch (1992) indicate that while advection influences SSTs along the polar front at ~40° in the central North Pacific, SSTs are primarily controlled by surface fluxes and entrainment. Thus, mixed layer models, which simulate vertical processes, appear to be well suited for studying the development of ocean surface temperature anomalies over most of the midlatitude oceans. These

models are also computationally efficient and easy to diagnose.

A one-dimensional ocean model developed by Gaspar (1988), which has been formulated with climate simulations in mind, is used to examine the influence of surface forcing and entrainment on ocean temperatures. The temperature of the mixed layer is controlled by surface energy fluxes, penetrating solar radiation, entrainment, and diffusion. Salinity in the model is specified according to climatology, since precipitation, which strongly influences salinity, is poorly known over the oceans. The MLD depends on the surface buoyancy forcing, wind stress, and penetrating solar radiation. If wind stirring and convective mixing associated with surface cooling cause the mixed layer to deepen via entrainment, the MLD is a time-dependent variable. Under stable conditions, the mixed layer re-forms closer to the surface, entrainment is set to zero, and the MLD is computed as a diagnostic by assuming a balance between mechanical turbulence and buoyancy forcing. When the mixed layer shallows, the temperature profile is adjusted according to Adamec et al. (1981), in order to conserve both heat and potential energy. The entrainment equation [Eq. (50) in Gaspar 1988] has seven constants; Gaspar calibrated these constants from observations and from the third-order turbulence closure model of André and Lacarrère (1985). We have used these parameter values in all of the simulations at OWS P and C.

The region beneath the mixed layer is represented by a multilayer system, where heat is redistributed through convective overturning, vertical diffusion, and penetrating solar radiation. The vertical diffusion is calculated using a constant coefficient of 2×10^{-5} m s^{-2}, estimated from analyses of Pacific MBT data by White and Walker (1974). The absorption of solar radiation is parameterized following Paulson and Simpson (1977). The model contains 30 unequally spaced layers between the surface and 1000 m; 15 of the layers are within the first 100 m in order to adequately represent the summer thermocline. The temperature of layers that are entirely above the MLD are set to the mixed layer value, while the temperature of the water below the mixed layer, used in the entrainment calculations, is obtained directly from the layer in which the MLD resides. The model is numerically integrated using a 1-day time step. A more detailed description of a similar version of the model is given by Alexander (1992).

Surface heat and momentum fluxes derived from atmospheric measurements are used as boundary conditions for simulations at a Pacific and Atlantic station, P and C, respectively. The net surface energy flux, Q_{net}, may be written as

$$Q_{net} = Q_{sw} - Q_{lw} - Q_{sh} - Q_{lh}, \qquad (1)$$

where Q_{sw} is the incoming shortwave radiation, Q_{lw} is the outgoing longwave radiation, and Q_{sh} and Q_{lh} are the sensible and latent heat fluxes, respectively. Here Q_{sw} is computed according to a formula developed by Reed (1977), which depends on the solar radiation at the top of the atmosphere, the cloud fraction, and the surface albedo (obtained from Payne 1972). We chose this formulation because it was calibrated for the midlatitude oceans. Here Q_{lw} is computed using the formula of Isemer and Hasse (1987) and depends on the SST, air temperature, and cloud fraction. Following Large and Pond (1982) and Large et al. (1994), the sensible and latent heat flux and the wind stress (τ) are calculated using bulk aerodynamic formulas in which the energy exchange coefficients depend on wind speed and stability estimated from the air–sea temperature difference. The surface energy fluxes are computed using the mixed layer temperature from the model, which is assumed to be equal to the SST.

The Q_{net} anomalies in winter at P and C are dominated by Q_{lh} and Q_{sh}. In summer, Q_{sw} and Q_{lh} and Q_{sh} anomalies are of comparable magnitude. The Q_{lw} anomalies are of secondary importance.

In all of the simulations the mixed layer model is driven by daily average surface fluxes and an additional heating of the mixed layer to roughly approximate the mean influence of ocean heat transport. The terms in Eq. (1) are evaluated using daily meteorological observations from P and C. Climatological flux values are used to drive the model on days when fewer than six observations are available. Errors in the atmospheric forcing, including the parameterizations used to compute the surface fluxes, deficiencies in the mixed layer model, such as having a constant diffusion coefficient below the mixed layer, and the absence of horizontal processes in the ocean model, particularly heat advection, can all cause the simulated ocean temperatures to drift from observations. Thus, in order to obtain an accurate representation of the seasonal cycle in SST the surface heat fluxes have been adjusted, where the adjustment implicitly includes the effects of the annual cycle in the ocean circulation on the annual cycle of SST. We sought simple formulas that would produce reasonably accurate extended model simulations: a constant cooling of 16 W m^{-2} is added at each time step during the simulation at P, while forcing of the form: $\{6 + 45 \cos(\text{day})\}$ W m^{-2}, which repeats over each year, is included at C.

5. Model experiments

a. Idealized model simulations

As a first step, we have performed two idealized model experiments in which anomalous surface forcing, Q'_{net}, composed of sinusoidal functions, is added to the observed net surface heat flux at P. Q'_{net} heats the mixed layer in winter and cools it in the following spring in case 1, and vice versa in case 2 (Fig. 7). The magnitude of the winter forcing is chosen to be double

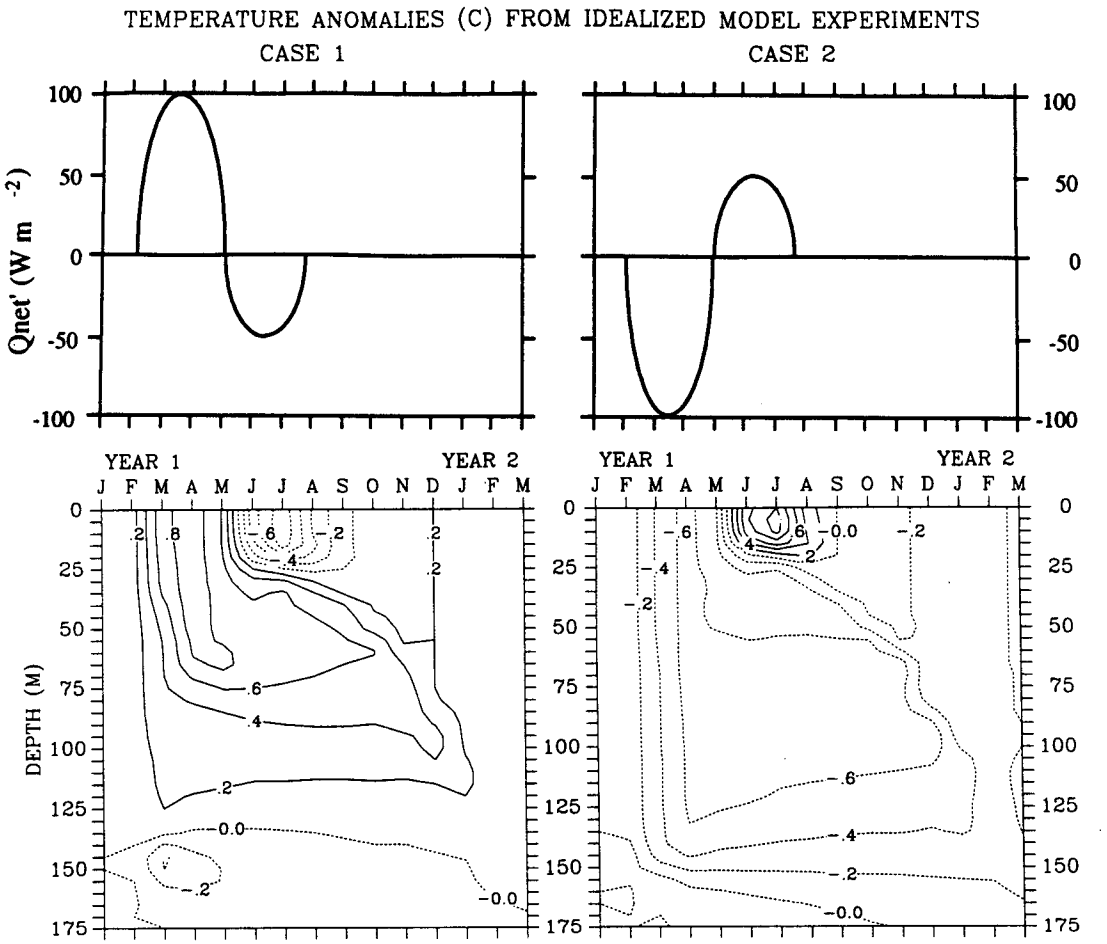

FIG. 7. Two cases of idealized anomalous atmospheric forcing (Q'_{net}) and the simulated ocean temperature response to the forcing (°C). Here Q'_{net} for case 1 is given by

$$100 \text{ W m}^{-2} \sin[2(\text{day} - 30)] \quad \text{for} \quad 30 < \text{day} < 120 \text{ of year 1}$$

$$50 \text{ W m}^{-2} \sin[2(\text{day} - 120)] \quad \text{for} \quad 120 < \text{day} < 210 \text{ of year 1}$$

$$0 \text{ W m}^{-2} \quad \text{for} \quad \text{all other days;}$$

the sign of Q'_{net} is reversed in case 2. The ocean temperature response is obtained by taking the difference between a 15-month simulation at OWS P with observed surface fluxes, and a second simulation in which the anomalous surface forcing is added to the observed forcing during the first year of the model run. The monthly temperature anomalies are unsmoothed.

the spring forcing since the observed standard deviation of Q'_{net} at P (not shown) is roughly twice as large in winter compared with spring.

The simulated ocean temperature anomalies that result from the anomalous surface forcing for case 1 and 2 are shown in Figs. 7a and 7b. The anomaly structure is similar in both cases: anomalies extend through the deep mixed layer in winter, persist within the seasonal thermocline in summer, and return to the surface in the subsequent winter. The temperature anomaly patterns in Fig. 7 resemble the observed anomaly correlation patterns, particularly at P and N (Fig. 6). Strong T' gradients form near the base of the mixed layer in summer as Q'_{net} creates temperature anomalies in the surface layer of opposite sign to those within the thermocline. By late fall/early winter, when $Q'_{net} = 0$, entrainment causes the sub-mixed layer temperature anomalies to return to the surface, though the anomalies are fairly small, ($|SST'| < 0.4$°C). The magnitude of the SST anomalies are partially damped by the surface energy fluxes: Q_{net} is computed using the model's mixed layer temperature (T_m) in the bulk aerodynamic formula; as T'_m increases (decreases) so does the release of sensible and latent heat from the ocean to the atmosphere.

There are some differences between the model's response to the two types of forcing. During winter, the negative temperature anomaly in case 2 extends

roughly 25–50 m deeper into the ocean compared with the positive anomaly in case 1. The maximum anomaly, which exceeds 0.8°C, extends over the upper 75 m during April in case 1, while in case 2 the anomaly amplitude only reaches ~0.6°C as the cooling is spread over a greater depth. In summer, the SST anomalies reach −0.8°C and 1.0°C in case 1 and 2, respectively. The greater magnitude of T' in case 2 is related to the anomalously warm mixed layer and cold thermocline, which increases the stability, causing a relatively shallow mixed layer. Anomalous surface warming then acts over a smaller depth, enhancing T'.

b. *Model simulations at weatherships P and C*

More realistic mixed layer model simulations have been performed in which observed daily average atmospheric conditions are used as boundary values in a 30-year run at Pacific OWS P (1950–1979) and a 28-year run at Atlantic OWS C (1946–1973). (Note that the period of record of the surface meteorological data and the SSTs used for verification is ~6–12 years longer than that of the MBT temperature measurements.) These two stations were chosen because they have fairly long and complete surface and MBT records. The simulated and observed monthly SST anomalies at P and C are shown in Fig. 8. A close correspondence between the simulated and observed SST occurs at both stations, especially at P. The correlation between the observed and simulated SST′ (Table 2a) for all months is 0.86 at P and 0.68 at C.[2]

The model reproduces most of the observed interannual fluctuations at both P and C (Fig. 8), indicating that even on decadal timescales the atmosphere may force ocean temperature anomalies. However, the strong coupling between the atmosphere and ocean through the latent and sensible heat fluxes may constrain the model to remain close to the observed air temperature and thus the observed SST, regardless of the processes that actually control the SST evolution. For example, changes in the ocean circulation could lead to SST anomalies that would be communicated to the atmosphere via the surface fluxes. The observed atmospheric conditions, which are subsequently used to drive the ocean model, could then result in a realistic simulation of the SSTs. Thus, the simulated SST anomalies would appear to have been formed by the atmospheric forcing, when in reality they resulted from internal changes in the ocean. The sensitivity of the model results to the method used to compute the surface fluxes is examined in section 5c.

An additional, and perhaps more rigorous test of the model is to compare the simulated and observed MLD,

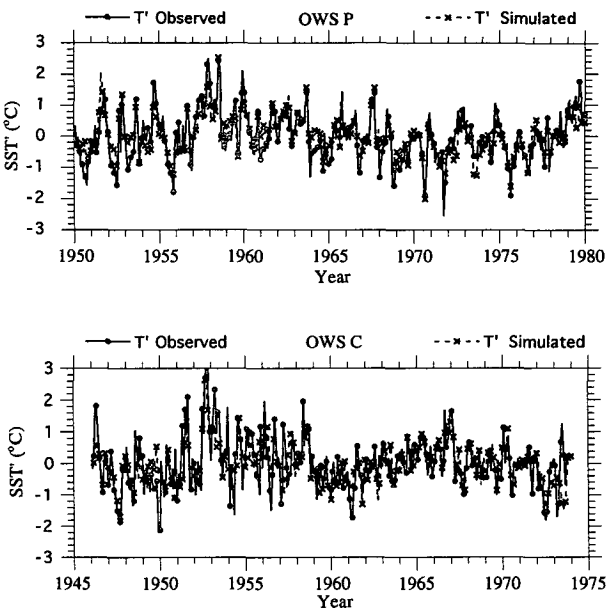

FIG. 8. Time series of the simulated (solid line) and observed (dashed line) monthly SST anomaly (°C) at OWSs P and C. Observed values are from surface marine reports; simulated values are from extended mixed layer model simulations. The data are smoothed with a 1-2-1 filter.

a quantity which is more independent of the method used to obtain the surface fluxes than the SST. At P, the correlation between the observed and simulated MLD exceeds 0.47 during each month and 0.68 over all the months (Table 2b). At C, the correlation exceeds 0.45 except for the months of January, February, March, and May. As the MLD anomalies from one year to the next are nearly uncorrelated, a correlation value exceeding ~0.45 is significant at the 95% level. Thus, the model shows significant skill in simulating the MLD during all months at P and during 8 of the 12 months at C.

There are several difficulties in comparing the observed and simulated mixed layer depths. Observed MLDs are estimated from temperature profiles, the only data available from the BTs, while in the model they depend on both the temperature and salinity. Levitus (1982) indicated that salinity can have an important influence on the depth of the mixed layer. In addition, the observed MLD is a somewhat arbitrary diagnostic, estimated here as the depth at which the subsurface temperature is 0.5°C colder than the SST. Changing the SST − T_{MLD} threshold to 0.1°C, as is used in some studies, influenced the correlation between the observed and simulated MLD, especially in winter. In late winter, the observed MLD may be deeper than the MBT record, which could also explain why the correlations between the observed and simulated MLD are not significant during January–March at station C.

[2] The correlations for all months between SST′ obtained from the MBT, instead of from the surface data, are 0.85 at P and 0.54 at C. The correlations decrease with depth and have values of ~.60 at P and ~.47 at C between 50 and 100 m.

TABLE 2. Monthly correlations between (a) the observed SST and simulated mixed layer temperature and (b) the observed and simulated MLD.

OWS	Jan	Feb	Mar	Apr	May	Jun	Jul	Aug	Sep	Oct	Nov	Dec	Total
						(a) SST							
P	0.70	0.65	0.68	0.81	0.86	0.89	0.86	0.91	0.92	0.95	0.91	0.73	0.86
C	0.76	0.82	0.58	0.61	0.47	0.66	0.66	0.87	0.83	0.62	0.53	0.49	0.68
						(b) MLD							
P	0.63	0.61	0.53	0.68	0.48	0.66	0.64	0.80	0.84	0.53	0.88	0.43	0.58
C	0.28	0.08	0.40	0.56	0.40	0.56	0.71	0.55	0.51	0.55	0.47	0.62	0.34

Following the observational analyses, the model results are correlated over depth and time to examine the seasonal dependence of the anomalous thermal structure in the upper ocean. Contemporaneous correlations between the monthly surface and subsurface temperature anomalies from the model simulations at P and C are shown in Fig. 9. The model contains a strong seasonal cycle in MLD indicated by large correlation values ($r > 0.8$) extending from the surface to beyond 100 m in winter but confined to less than 30 m in summer. In general, the model results at P and C (Fig. 9) bear a very close resemblance to the observed correlation patterns (top two panels in Fig. 4). The model is able to reproduce the negative correlations between SST′ and T' in the seasonal thermocline at both stations, and the difference in the anomaly correlation structure between the two stations: the negative values descend with time during the fall at P while they are confined to July and August around at C. However, some differences are apparent between the simulated (Fig. 9) and observed (Fig. 4) correlation fields. The magnitude of the negative correlations is slightly larger in the model compared with observations at P. In addition, large positive correlation values in the model are too deep (shallow) in winter at P (C). The differences between the model and data results may be due to (i) model deficiencies, such as the absence of temperature advection and predicted salinity; (ii) errors in the surface flux formulas; and (iii) the disparity in the record lengths; that is, the MBT data records at P and C are about two-thirds as long as the model simulations. However, the model results still differed from the observations when we computed the correlations with the same months that were used in the MBT data analyses.

Lead–lag correlations from the simulated temperature anomalies are shown in Fig. 10. The correlations are computed using the same base points as in the observational analyses, 50 m (80 m) during August at P (C). The correlation patterns obtained from the model integrations (Fig. 10) are similar to the observed patterns (Fig. 6) in that T' in the summer thermocline is well correlated with T' in the surface layer in the preceding and following winters but poorly correlated with the concurrent T' in the surface layer. Model deficien-

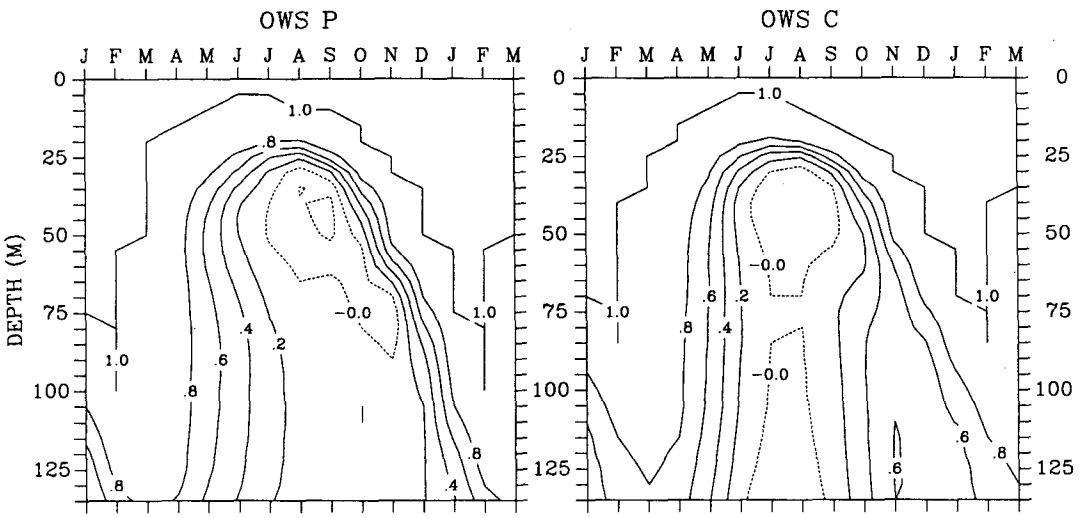

FIG. 9. Concurrent correlations between simulated monthly anomalies of SST and temperatures from the surface to 135 m in 5-m increments at P and C.

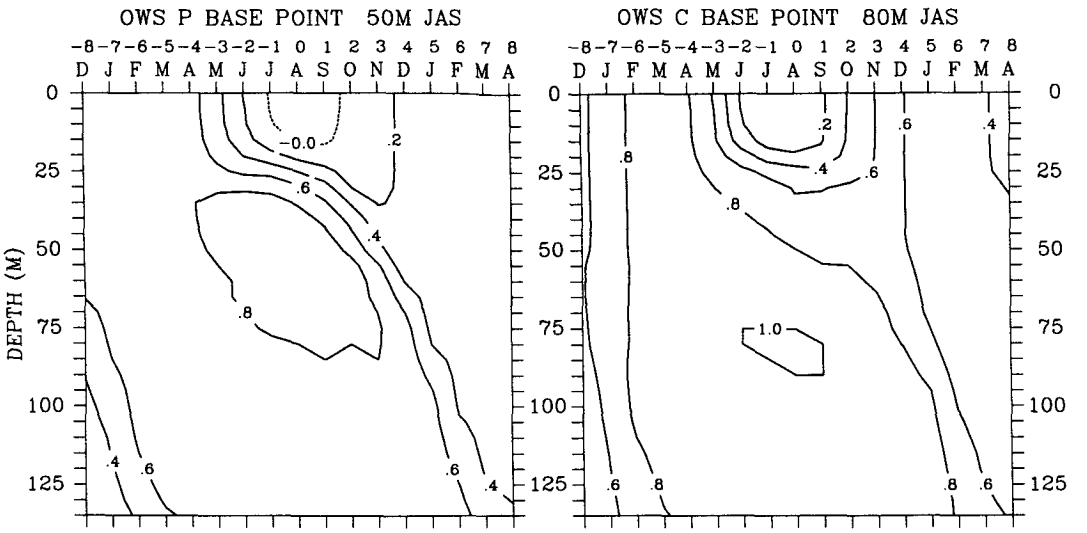

FIG. 10. Simulated lead–lag correlations between the temperature anomaly beneath the summer mixed layer (base point) and temperature anomalies in 5-m increments for the previous and following eight months. The data have been smoothed using a 3-month running mean; the middle month of the 3-month mean is shown at the top of each panel. The base points are 50 m in August at P and 80 m in August at C.

cies can also be noted. The MLM overestimates (underestimates) the correlations between T at the base point and the SST in the preceding (following) winter at both P and C. In addition, the correlation minimum ($r < 0.4$) observed during September–December around 75 m at P (Fig. 6) is not present in the model (Fig. 10). The simpler structure in the simulated compared with the observed anomaly correlation fields is due in part to the assumption of a single uniform mixed layer and the simple treatment of the ocean beneath the mixed layer in the model. Nevertheless, the model results suggest that anomalies created at the surface in winter/spring are stored below the mixed layer in summer and return to the surface in the following winter.

Some insight into the mechanisms determining the recurrence of SST anomalies is obtained from analysis of the equation for the anomalous mixed layer temperature, T'_m:

$$\rho c\left\{\mathrm{MLD}\,\frac{\partial T_m}{\partial t}\right\}' = \underset{\text{(I)}}{Q'_{\text{net}}} + \underset{\text{(II)}}{\rho c\{w_e(T_b - T_m)\}'} - \underset{\text{(III)}}{Q'_{\text{psw}}} + \underset{\text{(IV)}}{\rho c\kappa \frac{\partial T'}{\partial z}}, \quad (2)$$

where ρ is the density, c the specific heat, t time, κ the thermal diffusion coefficient, z the vertical coordinate, and the rest of the model variables are defined in Fig. 1. The processes controlling T_m are the net surface energy flux, Q_{net}, (I) and the heat flux due to entrainment, Q_{we}, (II), the penetrating solar radiation, Q_{psw}, (III) and the vertical diffusion at the base of the mixed layer (IV). The anomalous temperature tendency in the model is primarily controlled by Q'_{net} and Q'_{we}. Figure 11 shows the regression of anomalous fluxes Q'_{net} and Q'_{we} on $(\overline{\mathrm{MLD}}\,\partial T'_m/\partial t)$, over the course of a year from the extended runs. In terms of their contribution to $(\overline{\mathrm{MLD}}\,\partial T'_m/\partial t)$, Q'_{net} dominates Q'_{we} during November–May, whereas the reverse is true during August–October. In late winter/early spring Q'_{net} is large because strong winds coupled with large air–sea temperature differences lead to large sensible and latent heat flux anomalies. In contrast, the entrainment has little impact on the mixed layer temperature in late winter/early spring since w_e is small as the mixed layer has stopped deepening, and $T_b - T_m$ is at a minimum (Fig. 3). Thus, ocean temperature anomalies created by surface energy fluxes in winter and early spring can be returned to the surface layer by entrainment in fall.

c. *Sensitivity studies*

Given the uncertainty in the parameterizations incorporated in the mixed layer model and the wide variety of methods available to compute the atmospheric forcing, questions arise concerning the robustness of the re-emergence mechanism in the MLM. Here we examine the sensitivity of the model results to changes in (i) the ocean temperature used to compute the surface fluxes, (ii) the coefficients used in the bulk aerodynamic formula, and (iii) the diffusion rate at the base and below the mixed layer.

In the model results presented previously the surface fluxes were computed using the model's mixed layer temperature in the bulk aerodynamic formula, which

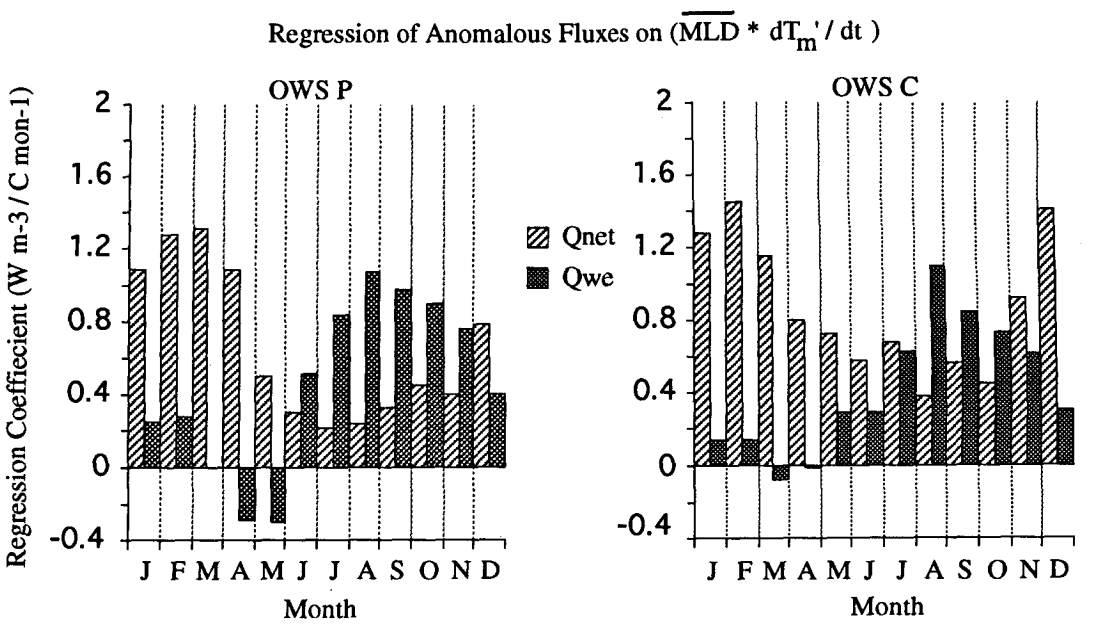

FIG. 11. The coefficients for the monthly average anomalous net surface energy flux, Q'_{net}, and entrainment heat flux, Q'_{we}, regressed on the mixed layer temperature tendency times the mean mixed-layer depth ($\overline{MLD}\ \partial T'_m/\partial t$) in W m^{-2} (m °C mon^{-1})$^{-1}$ from the mixed layer model simulations at OWS P and C.

constrains the simulated SST′ to follow the observed air T', and thus the observed SST′ (discussed in section 5b). A new 30-year simulation at OWS P has been performed where the surface fluxes are now computed with the observed SST. For clarity, we call simulations computed with observed SSTs, one way forced (OWF), while those computed with the model's SST are called partially coupled (PC). The results from a lead–lag correlation analyses of the OWF run, again with 50 m during July as the base point, are shown in Fig. 12a. As in the PC simulation (Fig. 10), the correlation between the temperature anomaly at the base point and T' in the surface layer in the previous spring and following winter are relatively high, while the temperatures in the surface layer in summer are uncorrelated with T' at the base point. Surprisingly, the r values in the OWF case more closely resemble those in the observations (Fig. 6) than the values obtained in the PC simulation. The surface correlation values range between 0.6 and 0.8 in the previous March through May and exceed 0.4 in the following December and January at the surface in both observations and the OWF simulation. A similar analyses has been performed on an OWF simulation at C (not shown); the results are similar to the PC simulation (Fig. 10) except that the correlation between T' in the seasonal thermocline and T' in the surface layer in the following winter are reduced from ~0.6 to ~0.4.

The second sensitivity experiment, also utilizes a 30-year OWF simulation at OWS P, but the surface fluxes are computed following Liu et al. (1979) instead of Large and Pond (1982). Liu et al. used a physical model of the surface and interfacial sublayers to obtain the coefficients in the bulk formula, while Large and Pond estimated these coefficients empirically. The results of the lead–lag correlation analyses forced by the fluxes computed following Liu et al. (Fig. 12b) are very similar to those computed following Large and Pond and are in good agreement with observations. We have also performed a simulation and correlation analysis where the flux coefficients are obtained from Ismer and Hasse (1987); the results (not shown) are similar to those in Figs. 12a and 12b.

The degree to which the late winter SST anomalies reemerge in the subsequent fall depends upon the rate of diffusion within the seasonal thermocline. If thermal anomalies diffuse downward rapidly in late spring and summer they may have little impact on the temperature of the mixed layer in the following fall. The vertical diffusion coefficient of heat (κ) in the real ocean is dependent on several processes, including shear and static stability, internal wave breaking, double diffusion, Langmuir cells, etc. (Nihoul and Jamart 1988; Large et al. 1994). Parameterizations for these and other local turbulent processes are still a subject of intensive research and uncertainty. However, the very large static stability within the summer seasonal thermocline strongly suppresses turbulence to a relatively small background level (Caldwell 1983; Gaspar et al. 1988; Price et al. 1987; Large, personal communication). Estimates of background diffusion obtained from data analyses, physical models, and tracer release experiments indicate $1 \leqslant \kappa < 5$ ($\times 10^{-5}$ m^2 s^{-1}) (Gregg and Sanford 1980; Osborn 1980; White and Bernstein 1981; Ledwell et al. 1993).

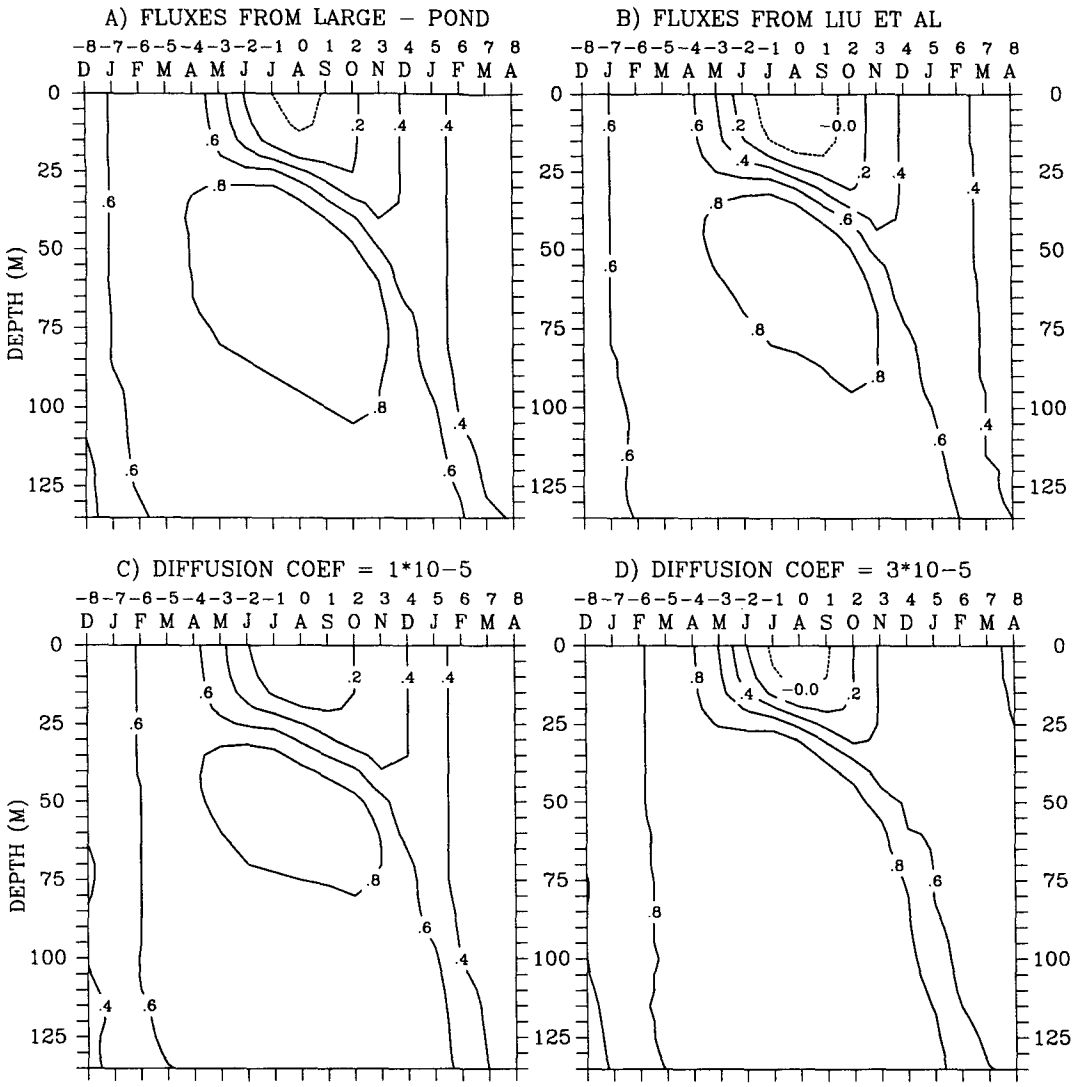

FIG. 12. Four sensitivity experiments of the simulated lead–lag correlations at OWS P using 50 m during July as the base point (as in Fig. 11). The surface fluxes in all four experiments are computed using the observed SST, termed one way forced. The simulation is performed using the flux formulas of (a) Large and Pond (1982) and (b) Liu et al. (1979). In (c) and (d) the fluxes are calculated as in (a), but the thermal diffusion coefficient, κ, has been changed from 2×10^{-5} $m^2 s^{-1}$ to in (c) 1×10^{-5} $m^2 s^{-1}$ and in (d) 3×10^{-5} $m^2 s^{-1}$.

In the third sensitivity study, we examine the impact of changing κ beneath the mixed layer on the re-emergence mechanism. Lead–lag correlation analyses performed on an OWF 30-year simulation at P, using κ values of 1×10^{-5} and 3×10^{-5} $m^2 s^{-1}$, are shown in Figs. 12c and 12d, respectively. The simulations use the flux formulation of Large and Pond, so a direct comparison can be made with the run shown in Fig. 12a where $\kappa = 2 \times 10^{-5}$ $m^2 s^{-1}$. Comparing panels a, c, and d in Fig. 12 indicates that increasing κ tends to enlarge the area of highest correlation ($r > 0.8$), reduces the correlation between SST′ and T' at the base point in summer, and enhances the corresponding SST′ – T' correlation in both the previous and subsequent seasons. The impact of κ on the correlation pattern suggests that higher diffusion values increase the penetration of thermal anomalies into the thermocline in late winter and spring, reducing the amount remaining in the surface layer by June. Some of this water spreads downward into the permanent thermocline but a substantial amount returns to the surface in the following winter. Comparing the correlation structure in Figs. 12a–c to the observed structure shown in Fig. 6 suggests that simulations with a thermal diffusion rate of between 1 and 2 ($\times 10^{-5}$ $m^2 s^{-1}$) beneath the mixed layer appear to best match observations, in agreement with Martin (1985) and Gaspar et al. (1988).

6. Summary and discussion

Mechanical bathythermographic data and mixed layer model simulations are used to examine the subsurface temperature structure at ocean weather stations in the North Atlantic and North Pacific. We employed correlation analyses as the primary tool for examining variations in temperature associated with the seasonal cycle. Concurrent correlations between the surface and subsurface temperature anomalies in both the data and model indicate that the penetration of temperature anomalies into the ocean is closely tied to the seasonal cycle in mixed layer depth: high correlations extend to relatively deep (shallow) depths in winter (summer). In summer, small negative correlations between SST anomalies and temperature anomalies in the seasonal thermocline likely result from changes in static stability caused by the vertical structure of the anomalies. For example, if the deep mixed layer is cooled in winter and the cold water persists beneath the shallow mixed layer in summer, then the stability is increased across the base of the mixed layer. This acts to shallow the mixed layer and thus the normal heating in summer acts over a smaller depth, creating anomalously warm SSTs. Lead–lag correlations in both the data and the model indicate that temperature anomalies beneath the mixed layer in summer are associated with the temperature anomalies in the mixed layer in the previous winter/spring and following fall/winter but are unrelated or weakly opposed to the temperature anomalies in the mixed layer in summer. These results suggest that vertical mixing processes allow ocean temperature anomalies created over a deep mixed layer in winter to be preserved below the surface in summer and reappear at surface in the following fall, confirming Namias and Born's hypothesis.

While the Namias–Born mechanism appears to play a role in the evolution of the observed SST anomalies at four of the six locations examined, the weak correlations indicate that other processes are also important. The dominant forcing mechanism of winter SST anomalies is the net surface energy flux (Q_{net}). Thus, the character of the seasonal autocorrelation of Q_{net} determines to a large extent the seasonal evolution of the SST anomalies. If Q'_{net} is out of phase between winter/spring and the following fall/winter, SST′ will also tend to be out of phase. For example, the correlation between Q'_{net} in spring (MAM) and fall/winter (NDJ) is −0.32 at P, indicating that there is a tendency for the surface fluxes to create an SST anomaly of the opposite sign from spring to the following winter. Conversely, the correlation between Q'_{net} in MAM and NDJ is 0.29 at C, suggesting that the surface fluxes enhance the positive correlations between SST′ in spring and the following winter. Model simulations at P and C indicate that entrainment has a large effect on the surface temperature in late summer and fall, a necessary condition for the re-emergence mechanism to occur.

Model simulations are also used to examine the extent to which diffusion and damping of SST anomalies by air–sea feedback impact the anomalous temperature structure in the upper ocean. Simulations in which the surface fluxes are computed with the model SSTs have temperature anomalies that are more strongly damped and constrained to closely follow the air temperature than those using the observed SSTs. We examined the mixed layer model's sensitivity to whether the model or observed SST was used to compute the surface fluxes; the coefficients used in the surface flux formulas; and the diffusion rate below the mixed layer. The sensitivity studies indicate that while the diffusion rate and method of obtaining the surface fluxes influenced aspects of the re-emergence mechanism, they did not change the fundamental pattern. We did not consider the impact of salinity on the density profile and the mixed layer depth. For example, warmer SSTs (associated with less dense water) would lead to enhanced evaporation, increasing the salinity and thus the density of the surface layer. Therefore, the influence of temperature and salinity anomalies may act to oppose each other with respect to the MLD and the depth to which anomalies penetrate.

Other processes may influence the Namias–Born mechanism, especially strong horizontal temperature advection associated with mean currents and synoptic eddies. The anomaly correlation pattern associated with the re-emergence mechanism is not found at stations D and H, located in the vicinity of the Gulf Stream. Miller et al. (1994) have recently looked for the re-emergence mechanism in a 19-year model simulation of the Pacific Ocean. The model, which includes mixed layer physics and Ekman and geostrophic currents, is forced by monthly anomalies of the observed heat, momentum, and turbulent kinetic energy fluxes for the years 1970–1988. Miller et al. found that the Namias and Born mechanism was weak over most of the area covered by the California Current and the Kuroshio Current and its extension into the central Pacific. However, the re-emergence mechanism did occur over sections of the North Pacific, including regions in the vicinity of OWS P and N. The influence of advection on the reemergence mechanism, the extent over which it occurs, and the magnitude of its impact on SSTs are subjects of future research.

Acknowledgments. The Atlantic and Pacific Ocean data were supplied by Steve Worley at the National Center for Atmospheric Research (NCAR) and Mary Hollinger at the National Oceanographic Data Center (NODC). We greatly benefited from discussions with Bill Large and Jan Morzel at NCAR. We would like to thank Martin Hoerling and David Battisti for their suggestions on the manuscript. The comments of two anonymous reviewers helped to improve the modeling portion of the manuscript. This work was supported by a grant from NOAA's Climate and Global Change Program.

REFERENCES

Adamec, D., R. L. Elsberry, R. W. Garwood, and R. L. Haney, 1981: An embedded mixed-layer-ocean circulation model. *Dyn. Atmos. Oceans,* **6,** 69–96.

André, J. C., and P. Lacarrerè, 1985: Mean and turbulent structures of the oceanic surface layer as determined from one-dimensional, third order simulations. *J. Phys. Oceanogr.,* **15,** 121–132.

Alexander, M. A., 1992: Midlatitude atmosphere–ocean interaction during El Niño. Part I: The North Pacific Ocean. *J. Climate,* **5,** 944–958.

Caldwell, D. R., 1983: Small scale physics of the ocean. *J. Geophys. Res.,* **21,** 1192–1205.

Davis, R. E., 1976: Predictability of sea surface temperature and sea level pressure anomalies over the North Pacific Ocean. *J. Phys. Oceanogr.,* **6,** 249–266.

——, 1978: Predictability of sea level pressure anomalies over the North Pacific Ocean. *J. Phys. Oceanogr.,* **8,** 233–246.

Frankignoul, C., 1985: Sea surface temperature anomalies, planetary waves, and air–sea feedback in the middle latitudes. *Rev. Geophys.,* **23,** 357–390.

——, and K. Hasselmann, 1977: Stochastic climate models. Part 2. Application to sea-surface temperature anomalies and thermocline variability. *Tellus,* **29,** 284–305.

——, and R. W. Reynolds, 1983: Testing a dynamical model for midlatitude sea surface temperature anomalies. *J. Phys. Oceanogr.,* **13,** 1131–1145.

Gaspar, P., 1988: Modeling the seasonal cycle of the upper ocean. *J. Phys. Oceanogr.,* **18,** 161–180.

——, Y. Gregoris, R. Stull, and C. Boissier, 1988: Long-term simulations of upper ocean vertical mixing using models of different types. *Small Scale Turbulence and Mixing in the Ocean,* J. C. J. Nihoul and B. M. Jamart, Eds., Elsevier Oceanography Series, No. 46, 169–184.

Gill, A. E., and P. P. Niiler, 1973: The theory of the seasonal variability in the ocean. *Deep-Sea Res.,* **20,** 141–177.

Gregg, M. C., and T. B. Sanford, 1980: Signatures of mixing from the Bermuda slope, the Sargasso Sea and the Gulf Stream. *J. Phys. Oceanogr.,* **10,** 105–127.

Haney, R. L., 1980: A numerical case study of the development of large-scale thermal anomalies in the central North Pacific. *J. Phys. Oceanogr.,* **10,** 541–566.

——, 1985: Midlatitude sea surface temperature anomalies: A numerical hindcast. *J. Phys. Oceanogr.,* **15,** 787–799.

——, B. H. Houtman, and W. H. Little, 1983: The relationship between wind and sea surface temperatures in the North Pacific Ocean. *Atmos.-Ocean,* **21,** 168–186.

Isemer, H.-J., and L. Hasse, 1987: *The Bunker Climate Atlas of the North American Ocean.* Vol. 2. *Air–Sea Interactions.* Springer-Verlag, 218 pp.

Kushnir, Y., and N.-C. Lau, 1992: The general circulation model response to a North Pacific SST anomaly: Dependence on time scale and pattern polarity. *J. Climate,* **5,** 271–283.

Large, W. G., and S. Pond, 1982: Sensible and latent heat flux measurements over the ocean. *J. Phys. Oceanogr.,* **12,** 464–482.

——, J. C. McWilliams, and S. C. Doney, 1994: Oceanic vertical mixing: A review and a model with a nonlocal boundary layer parameterization. *Rev. Geophys.,* **32,** 363–404.

Lau, N.-C., and M. J. Nath, 1990: A general circulation model study of the atmospheric response to extratropical SST anomalies observed in 1950–79. *J. Climate,* **3,** 965–989.

Lanzante, J. R., 1984: A rotated eigenanalysis of the correlation between 700 mb heights and sea surface temperatures in the Pacific and Atlantic. *Mon. Wea. Rev.,* **112,** 2270–2280.

Ledwell, J. R., A. J. Wilson, and C. S. Low, 1993: Evidence for slow mixing across the pychnocline from an open-ocean tracer release experiment. *Nature,* **364,** 701–703.

Leith, C. E., 1973: The standard error of time-averaged estimates of climatic means. *J. Appl. Meteor.,* **12,** 1066–1069.

Levitus, S., 1982: *Climatological Atlas of the World Ocean.* NOAA Prof. Paper No. 13, U. S. Govt. Printing Office, Washington D.C., 173 pp.

Liu, W. T., K. B. Katasaros, and J. A. Businger, 1979: Bulk Parameterization of air–sea exchanges of heat and water vapor including the molecular constraints at the interface. *J. Atmos. Sci.,* **36,** 1722–1734.

Luksch, U., and H. v. Storch, 1992: Modeling the low-frequency sea surface temperature variability in the North Pacific. *J. Climate,* **5,** 893–906.

——, ——, and E. Maier-Reimer, 1990: Modeling North Pacific SST anomalies as a response to anomalous atmospheric forcing. *J. Mar. Syst.,* **1,** 51–60.

Martin, P. J., 1985: Simulation of the mixed layer at OWS November and Papa with several models. *J. Geophys. Res.,* **90,** 903–916.

Miller, A. J., D. R. Cayan, and J. M. Oberhuber, 1994: On the reemergence of midlatitude SST anomalies. *Proc. 18th Annual Climate Diagnostic Workshop,* Boulder, CO, NOAA, 149–152.

Namias, J., and R. M. Born, 1970: Temporal coherence in North Pacific sea-surface temperature patterns. *J. Geophys. Res.,* **75,** 5952–5955.

——, and ——, 1974: Further studies of temporal coherence in North Pacific sea surface temperatures. *J. Geophys. Res.,* **79,** 797–798.

Nihoul, C. J., and B. J. Jamart, Eds., 1988: *Small-Scale Turbulence in the Ocean.* Elsevier Oceanogr. Ser. No. 46, 541 pp.

Osborn, T. R., 1980: Estimates of the local rate of vertical diffusion from disipation estimates. *J. Phys. Oceanogr.,* **10,** 83–89.

Palmer, T. N., and Z. Sun, 1985: A modelling and observational study of the relationship between sea surface temperature in the north-west Atlantic and the atmospheric general circulation. *Quart. J. Roy. Meteor. Soc.,* **111,** 947–975.

Paulson, C. A., and J. J. Simpson, 1977: Irradiance measurements in the upper ocean. *J. Phys. Oceanogr.,* **7,** 952–956.

Payne, R. E., 1972: Albedo of the sea surface. *J. Atmos. Sci.,* **29,** 959–970.

Pitcher, E. J., M. L. Blackmon, G. T. Bates, and S. Muñoz, 1988: The effects of North Pacific sea surface temperature anomalies on the January climate of a general circulation model. *J. Atmos. Sci.,* **45,** 173–188.

Price, J. F., E. A. Terray, and R. A. Weller, 1987: Upper ocean dynamics. *Rev. Geophys.,* **25,** 193–203.

Reed, R. K., 1977: On estimating insolation over the ocean. *J. Phys. Oceanogr.,* **7,** 482–485.

Salmon, R., and M. C. Henderschott, 1976: Large-scale air–sea interactions with a simple general circulation model. *Tellus,* **28,** 228–242.

Wallace, J. M., and Q. Jiang, 1987: On the observed structure of the interannual variability of the atmosphere/ocean climate system. *Atmospheric and Oceanic Variability,* H. Cattle, Ed., Roy. Meteor. Soc., 17–43.

——, C. Smith, and Q. Jiang, 1990: Spatial patterns of atmosphere–ocean interaction in the northern winter. *J. Climate,* **3,** 990–998.

Walsh, J. E., and M. B. Richman, 1981: Seasonality in the association between surface temperatures over the United States and the North Pacific Ocean. *Mon. Wea. Rev.,* **109,** 767–783.

White, W. B., and A. E. Walker, 1974: Time and depth scales of anomalous subsurface temperature anomalies at Ocean Weather Stations P, N, and V in the North Pacific. *J. Geophys. Res.,* **79,** 4517–4522.

——, and R. Bernstein, 1981: Large-scale vertical eddy diffusion in the main pycnocline of the central North Pacific. *J. Phys. Oceanogr.,* **11,** 434–481.

Zorita, E., V. Kharin, and H. v. Storch, 1992: The atmospheric circulation and sea surface temperature in the North Atlantic area in winter: Their interaction and relevance for Iberian precipitation. *J. Climate,* **5,** 1097–1108.